Nanoclay-mediated photocatalytic activity enhancement of copper oxide nanoparticles for enhanced methyl orange photodegradation

Idrees Khan[1] · Ibrahim Khan[2] · Muhammad Usman[3] · Muhammad Imran[4] · Khalid Saeed[1]

Abstract

Photodegradation of organic pollutants is considered to be the most suitable and cheaper techniques to counter the contamination issues. Metal nanoparticles are considered to be the most effective heterogenous photocatalysts for the photodegradation of organic pollutants. Besides, CuO oxide nanoparticles are well-known photocatalysts for photocatalytically degrading organic pollutants. Herein, we reported the synthesis of pure copper oxide nanoparticles (CuO NPs) and nanoclay-supported copper oxide nanoparticles (CuO/NC NPs) by facile chemical reduction technique for swift photodegradation of organic dye. The X-ray diffractogram (XRD) has demonstrated a typical monoclinic phase of CuO NPs. The morphological features via scanning electronic microscopy (FESEM) showed agglomerated morphology of CuO NPs with 372.57 ± 1.76 nm average particle size. The micrographs also revealed the homogenous dispersion of CuO NPs over NC surface in CuO/NC nanocomposite. A polydispersity index (PDI) of 0.39 presented slight variation in the particle size of CuO NPs, which is also supported by the results obtained from atomic force microscopy (AFM), FESEM and transmission electron microscopy (TEM). CuO/NC NPs demonstrated outstanding methyl orange degradation over a very short period of time under simulated light. Using CuO/NC NPs, about 97.18% and 95.96% dye degradations were achieved in merely 4 min, under UV and visible light, respectively. The excellent photodegradation efficacy of CuO/NC NPs can be attributed to the homogenous distribution of CuO NPs, which facilitates the generation of photoexcitons (electrons and holes), enhances charge transfer and minimizes the charge recombination. The NC induced the required photostability by providing sufficient space for NPs distribution.

1 Introduction

Organic dyes are the most renowned chemicals in industries as they are applied to substrates such as fibers to give them permanent color, which is able to resist fading upon exposure to light, sweat, water, oxidizing agents and microbial attack [1, 2]. Due to this extensive application

✉ Khalid Saeed
khalidkhalil2002@yahoo.com

1 Department of Chemistry, Bacha Khan University, Charsadda, Khyber Pakhtunkhwa, Pakistan

2 Centre of Integrative Petroleum Research, King Fahd University of Petroleum and Minerals, Dhahran 31261, Kingdom of Saudi Arabia

3 Centre of Research Excellence in Nanotechnology, King Fahd University of Petroleum and Minerals, Dhahran 31261, Kingdom of Saudi Arabia

4 H.E.J. Research Institute of Chemistry, International Centre for Chemical and Biological Sciences, University of Karachi, Karachi, Pakistan

and large-scale production, dyes are contemporary found in significant quantity in wastewater [3]. It is estimated that about 1–15% of synthetic textile dyes are discharged during manufacturing or processing operations into wastewater stream [4]. These dyes discharged from various industries including textile and food industries directly into water sources [5], which caused significant water pollution due to their carcinogenic nature [6]. Most of these dyes are toxic, non-biodegradable and carcinogenic due to their large size and complex structures [7], and hence, their accumulation could create potential risks and threats to aquatic and human life [8, 9]. Therefore, researchers are trying to overcome this issue by using various scientific approaches. These dyes are removed by various physical, chemical and biological methods like adsorption, precipitation, ozonization, reverse osmosis, flocculation and ultrafiltration [10]. Most of these methods are non-destructive, insufficient, and cause secondary pollution. Additionally, the well-established chemical methods are not economically feasible due to high chemical dosages and large scale of sludge production. Similarly, aerobic

decontamination is ineffective in case of stable dyes, while anaerobic decolorization of dyes generates carcinogenic aromatic amines [11]. Currently, various advanced oxidation processes such as sonocatalysis, ozonolysis, photo-Fenton, photocatalysis and photo electro-Fenton processes have emerged as popular techniques to degrade toxic compounds from wastewater [12]. Lately, heterogeneous semiconductor photocatalysis is employed to decompose dissolved organic dyes/pollutants in water [13–16]. In this process, metal nanoparticles (NPs) are used as heterogeneous photocatalysts for enhancing the process efficiency. Several metal NPs are reported as heterogeneous photocatalysts such as TiO_2 [12, 17], ZnO [18], $BiVO_4$ [19], WO_3 [20], Fe_2O_3 [21] and copper-based NPs [21, 22]. Though most of these NPs are found useful initially yet experienced some disadvantages when utilized in suspension. The major disadvantage includes NPs aggregation in suspension, which effectively influenced photocatalytic performance negatively, and impacted catalytic recovery. These problems can be overcome by immobilizing catalyst on a suitable support medium [23]. The support catalysts show enhanced decomposition rate as compared to unsupported, which are attributed to increased condensation of organic substrates on the supported catalyst by adsorption and the reduction in electron-hole recombination process on the surface [24]. Researchers reported various support media in order to retard the NPs aggregation, which include graphene [10] polyethersulfone matrix [23], ceramics [25], carbon nanotubes [26], activated carbon [27], zirconia [28], etc.

Copper is one of the cheapest and has a wide range of applications like gas sensors [29], lithium-ion electrode and batteries [30, 31], antibacterial agent [32, 33], field emission devices [34], dye-sensitized solar cells [35], adsorption [36, 37] and heterogeneous catalysts [38, 39]. Moreover, copper-based materials are also found useful in various photocatalytic applications, lately such as photoconversion of hydrocarbons into less toxic materials [1]. Copper-based semiconductors exhibited a narrow band gap, which can be tuned precisely by employ various techniques. Therefore, they have been used widely as a powerful heterogeneous photocatalysts [40].

In the present study, we are reporting the synthesis of pure copper oxide nanoparticles (CuO NPs) and nanoclay-supported copper oxide nanoparticles (CuO/NC NPs) by chemical reduction method using NaOH as a reducing agent. The as-synthesized photocatalysts are employed for methyl orange (MO) photodegradation. MO is a water soluble azo dye widely used in printing, textile, paper manufacturing, food, pharmaceutical industries, etc. [41]. It is highly toxic and acute exposure to it can cause shock, vomiting, increased heart rate, cyanosis, quadriplegia, and jaundice and tissue necrosis in humans [42]. The maximum degradation in our

study is achieved in a mere four minutes time with sufficient photocatalyst recovery. The current study has reported the shortest degradation time to the best of our knowledge.

2 Materials and methods

2.1 Materials

Sodium hydroxide was supplied by Sigma-Aldrich. Methyl Orange was supplied by English Medication House Ltd., London, United Kingdom. $CuCl_2 \cdot 2H_2O$ was supplied by Sigma-Aldrich. All the chemicals are used as received.

2.2 Synthesis of NC/CuO composite and CuO NPs

100 mL solution of $CuCl_2 \cdot 2H_2O$ (0.5M) and 4 g nanoclay (NC) were added to a volumetric flask. The mixture is stirred and sonicated (10 min) until uniform mixing achieved. The obtained mixture is then basified by dropwise adding NaOH (2M) solution until the mixture pH attained 9 under constant stirring. The reaction mixture was refluxed for 4 h with constant stirring. It is identified by characterization techniques that CuO NPs are successfully synthesized after the reduction of $CuCl_2 \cdot 2H_2O$ salt precursor according to Eqs. (1) and (2). The obtained solution (gray color) is cooled, filtered and washed many times with distilled water to remove unwanted and unreactive impurities. The obtained $Cu(OH)_2$ NPs was then heated at 150 °C for converting to CuO/NC NPs and then stored. The same procedure was followed for the synthesis of CuO NPs without adding NC.

$$CuCl_2 + NaOH \longrightarrow Cu(OH)_2 + NaCl \qquad (1)$$

$$Cu(OH)_2 \longrightarrow CuO + H_2O. \qquad (2)$$
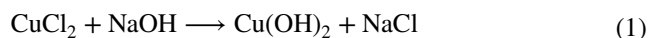
2.3 Photodegradation of methyl orange dye

The CuO/NC NPs and CuO NPs were tested for the photodegradation of MO dye as a function of several parameters. 10 mL MO dye solution (30 ppm) was taken in a beaker and a known quantity of photocatalyst was added to it. The mixture was then kept in dark for 30 min in order to attain adsorption–desorption equilibrium. The mixture was sonicated for 2 min and irradiated under simulated UV (254 nm, 15 W) or visible light for a specific irradiation time. After completion of the reaction time, the catalyst was separated through centrifugation (12,000 rpm/min) (Sigma, Model 1–14). The photodegradation study was conducted by UV–Visible spectrophotometer (Shimadzu 1800, Japan). The %degradation of MO dye is calculated by using the following formula:

$$\text{Degradation rate (\%)} = \frac{C_o - C}{C_o} \times 100 \qquad (3)$$

$$\text{Degradation rate (\%)} = \frac{A_o - A}{A_o} \times 100, \qquad (4)$$

where C_o is the initial dye concentration, C is the dye concentration after UV irradiation, A_o shows initial absorbance, and A shows the dye absorbance after UV irradiation.

2.4 Characterizations

The morphological study of photocatalysts was performed by SEM (LA-6490, JEOL Japan, in the energy range of 0–20 keV), AFM (5500, Agilent, Santa Clara, USA) and TEM (TEM of the samples was taken using a JEOL system (JEM2100F) operating at an acceleration voltage of 200 kV. Each sample was prepared from dry sample in ethanol followed by sonication for 30 min. A droplet (5μL) of dilute suspensions was deposited in a 300-mesh pure carbon-supported grid and then kept in vacuum station for 1 h for further drying before analysis. The particle size, PDI and zeta potential were determined by Zetasizer (ZS-90 Malvern Instruments, Malvern, UK). The crystal structure and different functional groups were detected through X-Ray Diffraction (D8-advance instrument, Bruker AXS Ltd., Germany) and Fourier Transform Infrared (Nicolet Nexus 470, Thermo Electron Co., USA). The photodegradation study was monitored by UV/Visible spectrophotometer (Shimadzu 1800, Japan).

3 Results and discussion

3.1 Morphological and elemental composition and mapping study

AFM, SEM and TEM microscopic details were obtained for NC, CuO/NC NPs and CuO NPs. Figures 1a–c and 2a–c show the 3D AFM and SEM images of NC, CuO/NC and CuO NPs, respectively. Figures 1 and 2a show that NC has a rough surface and a typical clay morphology is observed. Figures 1b and 2b demonstrate CuO NPs decoration over the NC surface with reasonable particle distribution. Moreover, Figs. 2 and 3c represent neat CuO NPs, which are mostly agglomerated with irregular geometry both in spherical and cylindrical form.
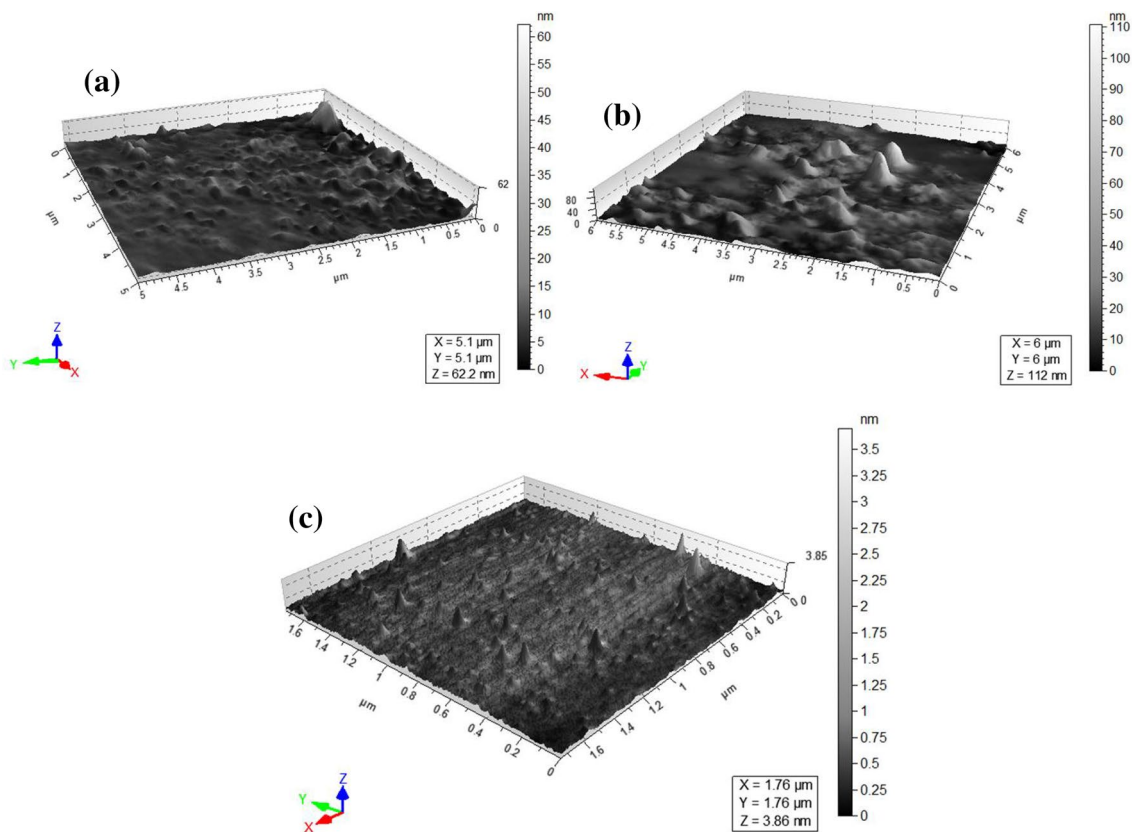

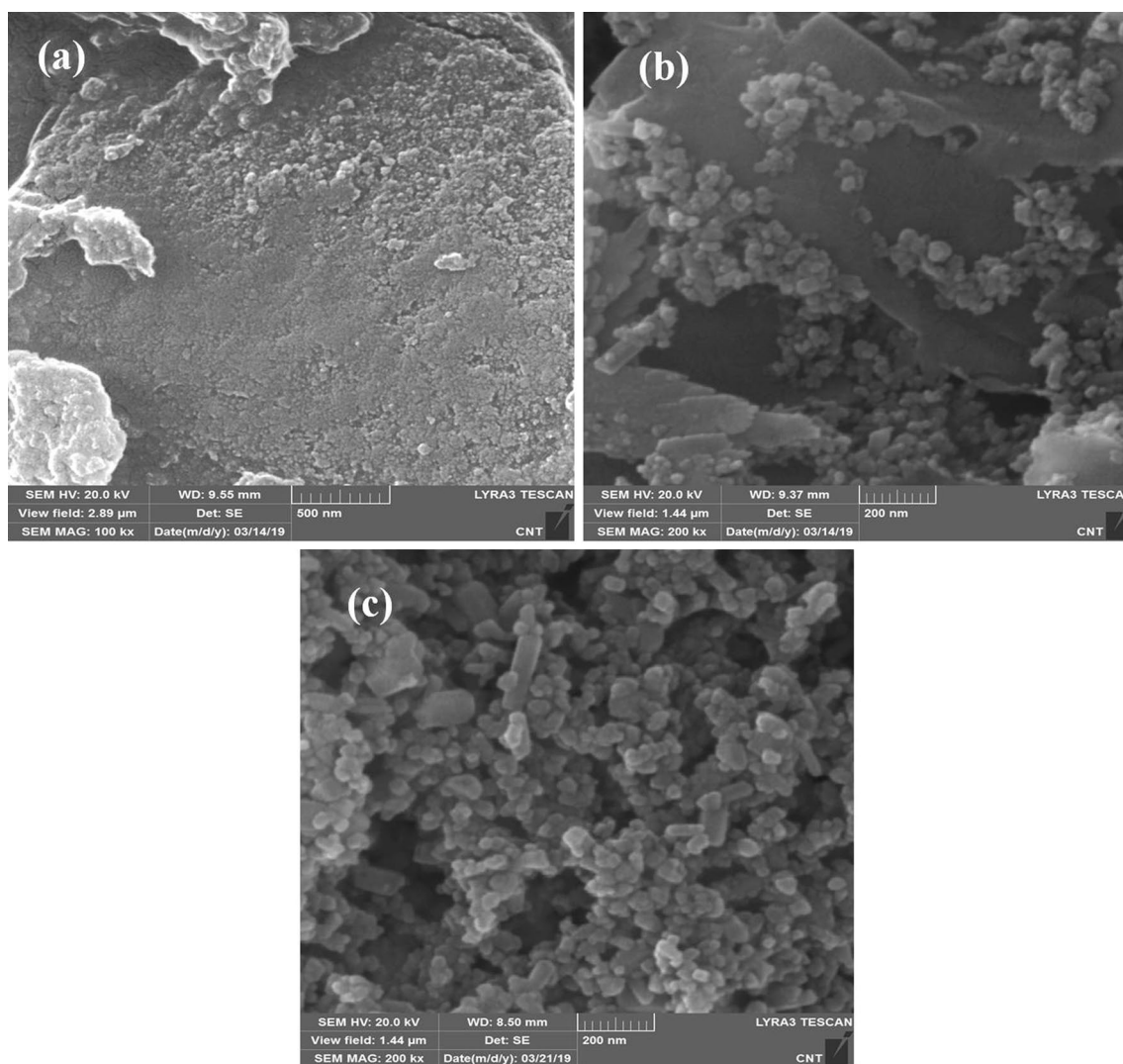**Fig. 1** AFM 3D images of **a** NC, **b** CuO/NC NPs and **c** CuO NPs

Fig. 2 SEM images of **a** NC, **b** CuO/NC NPs and **c** CuO NPs

The composite CuO/NC NPs are further deeply investigated through TEM in order to study its phase, size and particles intercalation and represented in Fig. 3. Figure 3a–d shows the TEM images of NC mediated CuO NPs at different magnifications. The images show that CuO NPs are well dispersed on the NC surface and also deposited in their gaps. Higher magnified images of TEM (b and c) verify the spherical structure of CuO with an average size of about 10–20 nm and are well distributed over the particles of NC. Further magnified TEM image (d) reveals the crystallographic plane of the monoclinic CuO and clearly revealing the heterojunction texture of nanosized CuO and NC.

The EDX spectra, elemental composition and elemental mapping of CuO NPs and CuO/NC NPs are consolidated in Figs. 4 and 5, respectively. Figure 4a displays known peaks for Cu and O and its % composition, which confirms the synthesis of oxide NPs. Figure 4b and c shows

the mapping results of Cu and O, respectively, and support the EDX results. Figure 5a shows characteristic peaks for Si (due to NC), Cu and O and their % composition (table in Fig. 5a), revealing the formation of CuO/NC composite. Figure 5b–d supports the EDX results (Fig. 5a) and the mapped area shows a significant distribution of CuO NPs on the NC surface.

3.2 XRD analysis

Figure 6 shows the XRD pattern of the NC, CuO/NC NPs and CuO NPs. The peaks indicate that Cu nanoparticles are present both in pure and oxide form. The peak observed in XRD pattern at 2θ values of 43° and 50.7° in the CuO/NC NPs and CuO NPs represent fcc structure of pure copper. The strong XRD pattern centered at 32°, 36° and weak patterns at 39°, 49° and 62° indicated the formation of highly
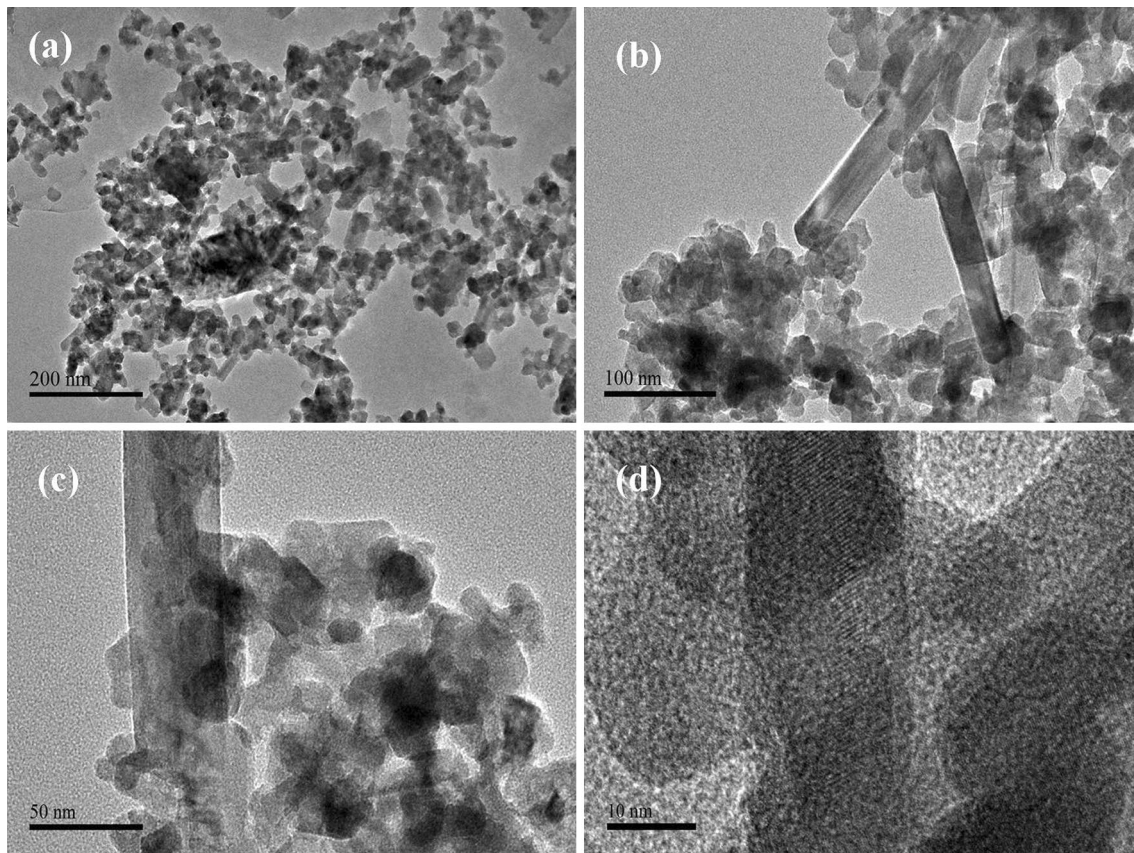
Fig. 3 TEM images of CuO/NC NPs at different magnifications

pure single-phase CuO with a monoclinic structure [40, 43]. The figure also contains the standard XRD pattern of CuO nanoparticles in the corner. The peaks observed at 33° and 40° can be assigned to $Cu(OH)_2$ which are not converted into CuO during heat treatment [44]. The existing of hydroxide could be attributed to surface moisture absorption from the exposed atmosphere. The peaks observed in the NC are in good agreement with the available literature [45, 46].

3.3 FTIR analysis

FTIR analysis was performed to identify stretching and vibrating modes in as-synthesized sample, i.e., NC, CuO NPs and CuO/NC composite. The broad band in Fig. 7 at 3480 cm^{-1} and 617 cm^{-1} in the Cu spectrum represents the stretching frequency of –OH group of absorbed water present on the surface of copper NPs. Additionally, peaks observed at 480 cm^{-1}, 530 cm^{-1} and 580 cm^{-1} can be attributed to the Cu–O vibrations, which could be related to the synthesis of CuO nanoparticles. The stretching frequency at 3623 cm^{-1}and bending frequency at 915 cm^{-1} in NC spectra is for Al–Al–OH, while the band at 1627 cm^{-1} represents –H–O–H vibration. Weak peaks at 471 cm^{-1} and 523 cm^{-1} ascribed the presence of bonds such as

Si–O–Al and Si–O–Mg in NC. These peaks were merged with the peaks of Cu NPs in the composite CuO/NC NPs spectrum, which could be related to the incorporation of Cu NPs on the surface of NC. The other peaks observed in te NC are also reported in the literature.

3.4 Particle size and zeta potential

Figure 8 shows the size distribution plot of CuO NPs, which presents the average particle size 372.57 ± 1.76 nm, which is actually the hydrodynamic size of particles and measured from the DLS. The size of nanoparticles measured from DLS is much larger as compared with the size measured from AFM images, which might be due to the swelling of CuO NPs in an aqueous medium. The Cu NPs have a PDI of 0.39, which reveals medium variation in the Cu NPs particle size. The zeta potential of the CuO NPs is shown in Fig. 9, representing a surface charge of 16.5 ± 0.46 mV. Though the surface charge is significant for any physical interaction, yet it is weaker enough to repel the near particles and hence lead to agglomeration and lower photocatalytic activity, if used in pure form.
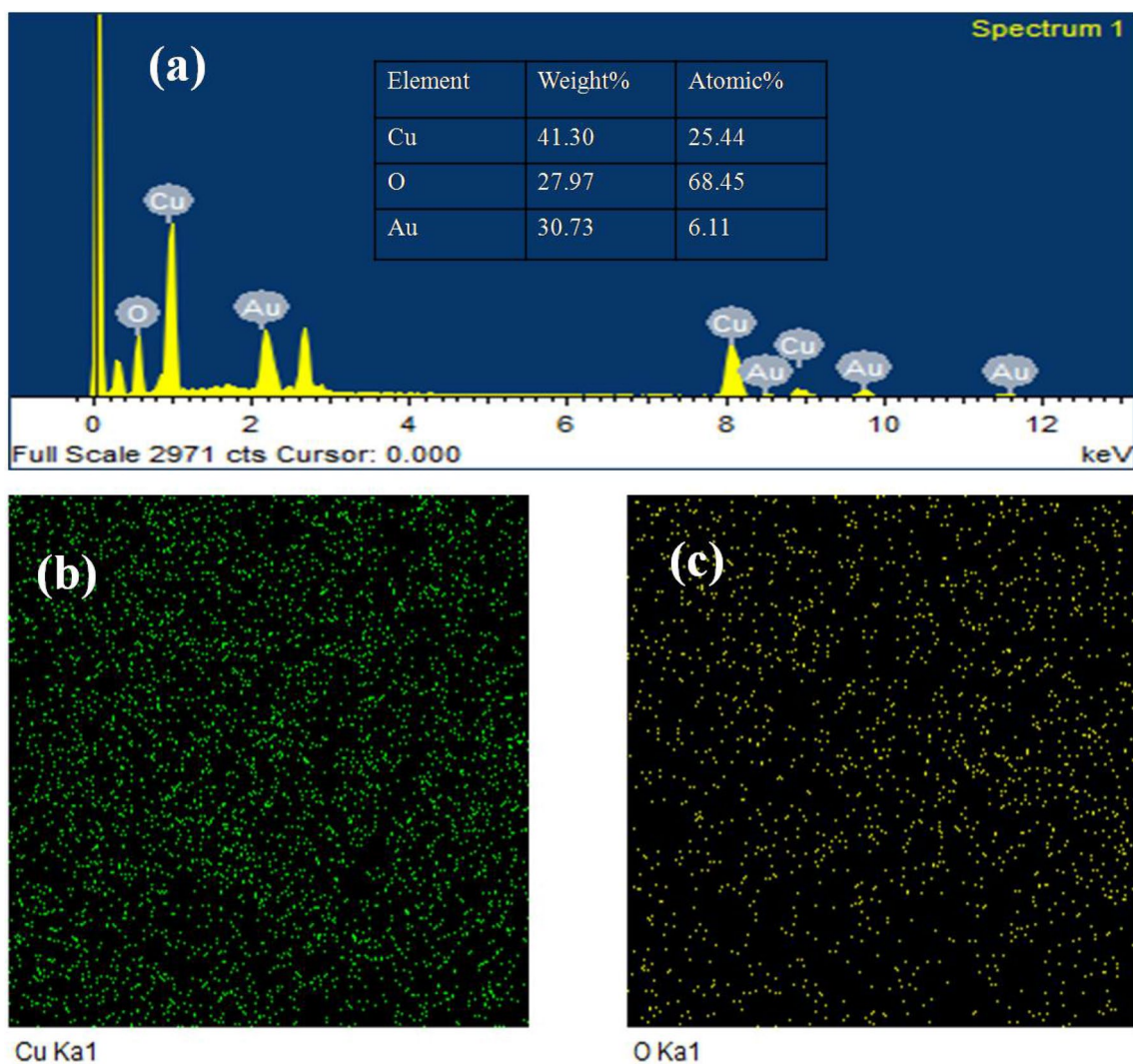
Fig. 4 **a** EDX analysis of CuO NPs, **b**, **c** elemental Mapping of CuO NPs

3.5 Photodegradation of methyl orange dye

The photocatalytic activity of nanoclay (NC), CuO NPs and CuO/nanoclay NPs (CuO/NC NPs) are tested for the photodegradation of methyl orange (MO) dye in aqueous medium under UV and visible light. Figure 9a–c shows the UV–Vis spectra of MO dye before reaction and acquired after different intervals of time of UV-light irradiation in the presence of NC, CuO/NC NPs and CuO NPs in an aqueous medium. The photodegradation of the MO dye was measured from its UV–Vis spectra, which gave a maximum absorbance peak at 465 nm. The intensity decrease is observed with increasing light exposure time because photodegradation decreases dye concentration. Figure 10 shows the digital photograph of MO dye photodegraded in the presence of NC (10a), CuO/NC NPs (10b) and CuO NPs (10c), respectively, as a function of irradiation time. Figure 11a displays the %degradation comparison of MO dye in the presence of NC, CuO/NC NPs and CuO NPs. Figures 9, 10 and 11a show that the photodegradation increases as irradiation time increases. The figures confirm that in the presence of NC only a small quantity of dye is removed as it can only adsorb dye. Similarly, the CuO/NC NPs and CuO NPs degraded dye efficiently but CuO/NC NPs are much effective than CuO NPs. The %degradation result shows that within 1 min NC decolorizes about 30.44% dye, which increases upto 43.41% dye by increasing irradiation time to 4 min. Such quantity of dye removed by NC is through adsorption as confirmed through its desorption study. The CuO/NC NPs are very effective and degraded 95.96% MO dye within 1 min, which increases to 97.18% by increasing irradiation time to 4 min. Similarly, CuO NPs degraded about 62.36% dye in 1 min, which increases slowly upto
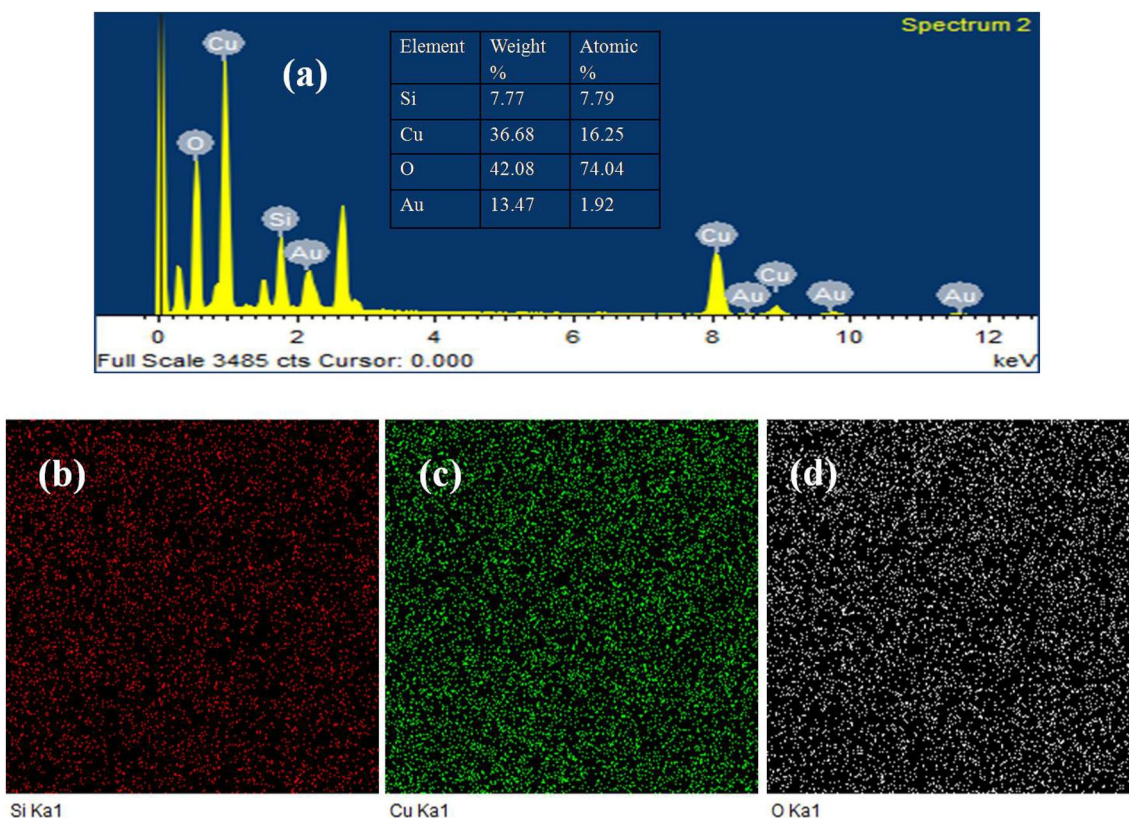
Fig. 5 **a** EDX analysis of CuO/NC NPs, **b**, **c** and **d** elemental mapping of CuO/NC NPs
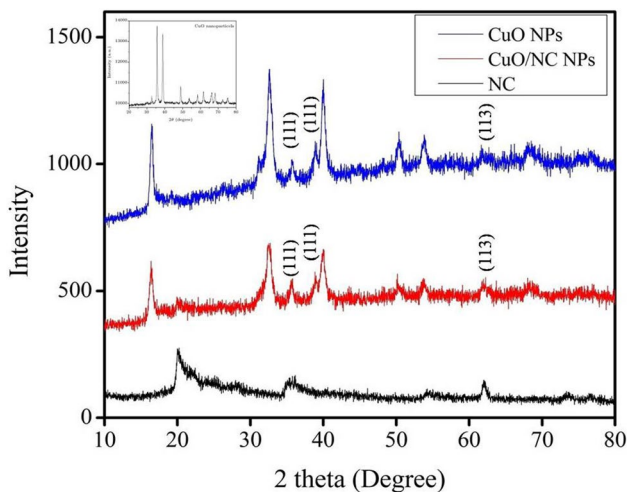

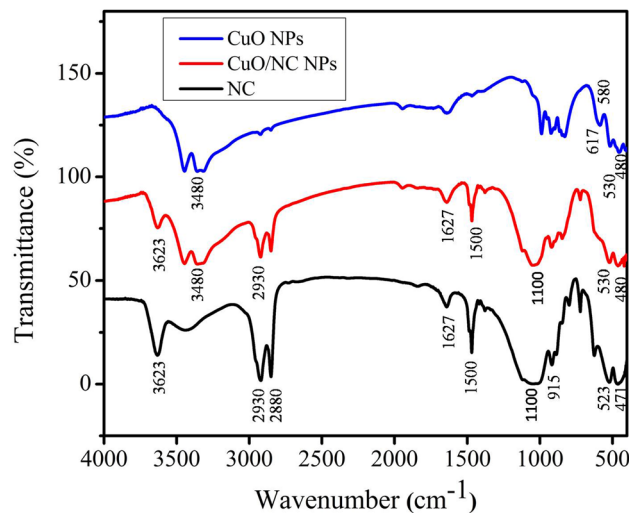**Fig. 6** XRD patterns of NC, CuO/NC NPs and CuO NPs

Fig. 7 FTIR spectra's of NC, CuO/NC NPs and CuO NPs

68.22% by increasing irradiation time to 4 min. Such enhance activity of the CuO/NC NPs than CuO NPs is due to uniform deposition of CuO NPs on the surface of NC, which increases CuO NPs surface area and its synergistic effect in reducing the recombining deficiency of created charges and quick dye adsorption on NC followed

by its rapid photodegradation by supported CuO NPs [47]. Various studies are also reported to enhance the activity of Cu NPs for efficient MO degradation by synthesizing supported/composite Cu NPs but at a relatively slower rate. For example, Gao et al. [48] synthesized porous Cu/ Carbon composites and CuO NPs and utilized for methyl
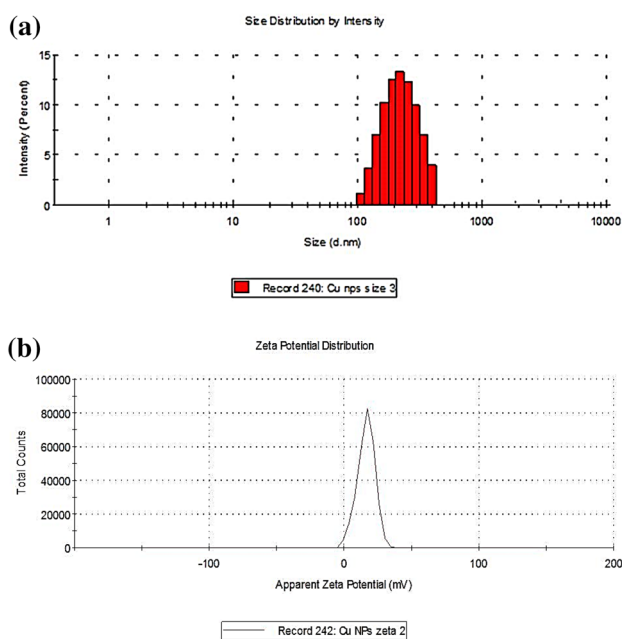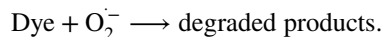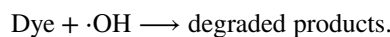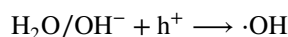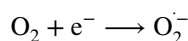
(a)

(b)

Fig. 8 **a** Size and size distribution plot of CuO NPs, **b** plot of total counts versus zeta potential (mV) of CuO NPs

orange photodegradation. Their results indicate that Cu/Carbon composites show remarkable high activity than CuO and degraded 80% dye within 120 min. Similarly, Sun et al. [49] synthesized Cu_2O octahedral and cubic microcrystals and it's composite with reduced graphene oxide for MO photodegradation and found that the photocatalytic activity of rGO/Cu_2O octahedral is 4 times faster than Cu_2O octahedrons and rGO/Cu_2O cubic. Their results indicate that Cu_2O cubes degraded 5% dye, Cu_2O octahedrons 17.6%, rGO/cubes 21%, while the rGO/octahedrons degraded about 81% within 2 h. As compared to these studies, the NC/Cu NPs degraded 97.18% in 4 min. Figure 11b shows a plot of lnCo/C versus irradiation time, which presents a linear relationship, indicating pseudo-first-order kinetics. The correlation coefficient (R^2) values were also presented in the graph. The photodegradation of MO dye by other photocatalysts in the literature are compared with our current study and are consolidated in Table 1.

The CuO/NC NPs are highly sustainable as compared to CuO NPs confirmed from its recyclable catalytic activity. Figure 12a shows the %degradation comparison of MO dye photodegraded by fresh and recycled (washed with distilled water and oven dried) CuO/NC NPs. The fresh CuO/NC NPs degraded 97.18% dye, while the recycled form degrades 89.72% dye within 4 min. Figure 12b represents the comparison of MO dye photodegraded by fresh and recycled CuO NPs. The fresh CuO NPs degraded 68.22% dye, while the recycled degraded 56.69% within 4 min. The results verified

that CuO/NC NPs are much sustainable and can be used several times as compared to CuO NPs.

The electron (e^-) from the valence band (VB) of NPs is excited to the conduction band (CB) when absorbed a light photon and create a positive hole (h^+) in the valence band. The VB electron reacts with O_2 and produces superoxide anion radical ($O_2{}^{\cdot-}$), while the positive hole reacts with H_2O molecule and generates hydroxyl radical (·OH). These both generated radicals are strong oxidizing agents, highly reactive and degraded dye molecules into simpler species [7]. The enhanced activity of CuO/NC NPs is attributed to the high surface area of CuO NPs, which is well dispersed on NC surface and its synergistic effect in quick dye adsorption on NC followed by its rapid photodegradation by supported CuO NPs. The possible reaction steps in this mechanism are summarized in the following equations.

$$NPs \longrightarrow NPs\ (e^- + h^+)$$

$$O_2 + e^- \longrightarrow O_2^{\cdot-}$$

$$H_2O/OH^- + h^+ \longrightarrow \cdot OH$$

$$Dye + \cdot OH \longrightarrow degraded\ products.$$

$$Dye + O_2^{\cdot-} \longrightarrow degraded\ products.$$

The proposed reaction mechanism can easily be understood from Fig. 13.

The photocatalytic activity of both photocatalysts is also studied in visible light under the same experimental conditions. Figure 14a represents %degradation of dye by CuO/NC NPs and CuO NPs under visible light. It was found that the NC-supported CuO NPs is also highly active under visible light and efficiently degraded MO dye as compared to CuO NPs. The results revealed that the CuO/NC NPs degraded 95.96% dye, while the CuO NPs degraded 62.59% dye within 4 min under visible light irradiation. Figure 14b and c shows the comparison of % degradation of MO dye under UV and visible light in the presence of CuO/NC NPs and CuO NPs, respectively. The figures display that the supported photocatalyst is active under both UV and visible light as compared to the unsupported photocatalyst.

3.6 Effect of tap water

The MO dye solution (30 ppm) was prepared in tap water and studied under the same experimental conditions and a decrease was observed in the photocatalytic activity of both the photocatalysts. Figure 15a represents the comparison of %degradation of MO dye in the presence of both photocatalysts in tap water under UV-light irradiation. Figure 15b and
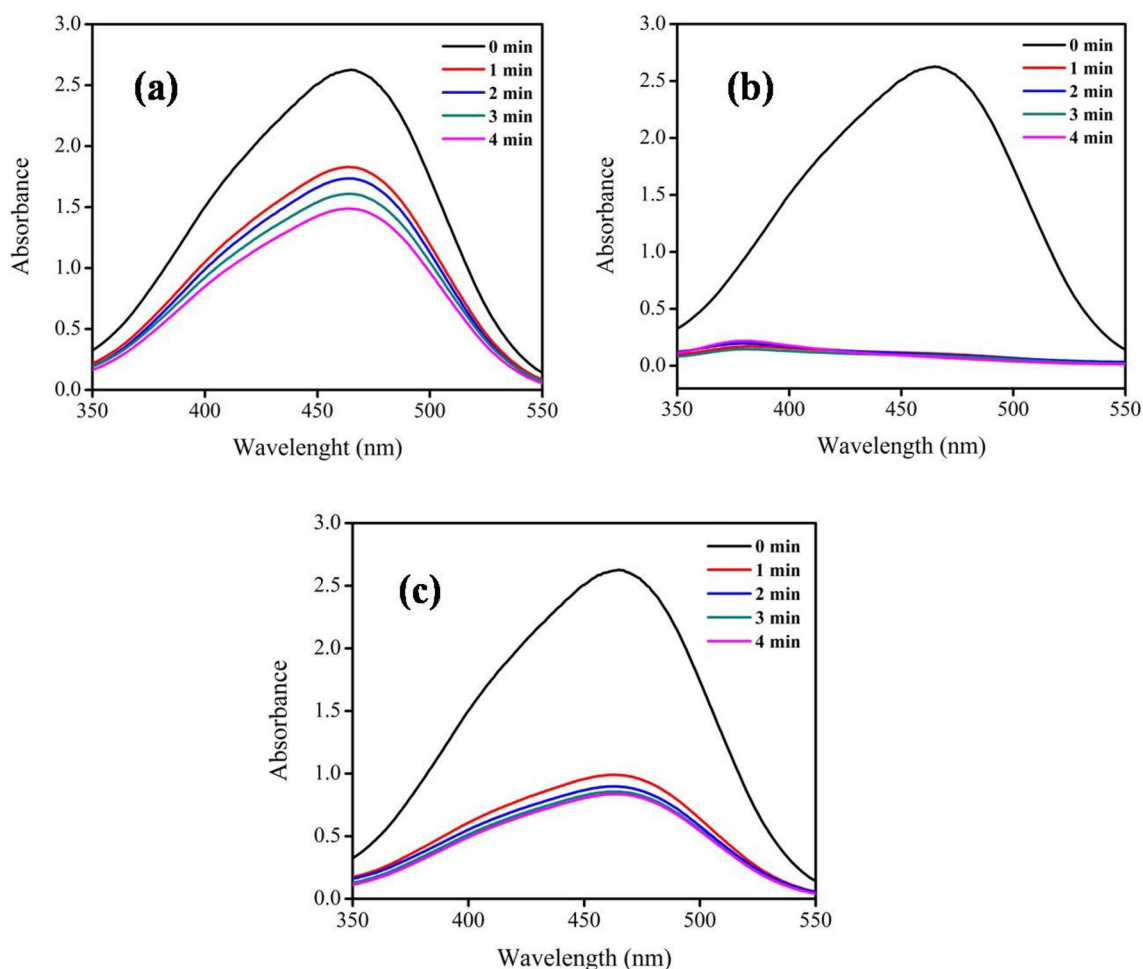
Fig. 9 UV–Vis spectra of MO dye before and after UV-light irradiation in the presence of **a** NC, **b** CuO/NC NPs and **c** CuO NPs

c shows the %degradation comparison of MO dye in distilled and tap water in the presence of CuO/NC NPs and CuO NPs photocatalyst under UV-light, respectively. It was observed that the CuO/NC NPs degraded 97.18% dye in distilled water and 47.33% dye in tap water within 4 min. Similarly, CuO NPs degraded 68.22% dye in distilled water and 23.4% dye in 4 min. The possible reason for such decrease in photocatalytic activity of the photocatalysts is due to the presence of inorganic, organic and metallic ions, which serve as competing species against the active sites of catalyst, hence reducing its activity [56].

3.7 Effect of catalyst dosage

Catalyst amount plays a vital role in dye degradation because changing amounts of catalyst provide a different number of active sites [57]. Different catalyst amounts (0.005, 0.010, 0.015, 0.020 and 0.025 g) were added to the dye solutions and their effect was studied and it was

concluded that increasing catalyst dosage up to a certain limit (0.015 g) increases photodegradation rate. Figure 16 shows the %degradation of MO dye in the presence of different dosages of CuO/NC NPs and CuO NPs in 1 min UV-irradiation time. Initially, 0.005 g of CuO/NC NPs degraded about 47.64% MO dye and increasing dosage to 0.015 g dye degradation increased to 94.9%, which is the optimum limit. Increasing beyond this limit, no significant enhancement is achieved and 0.02 and 0.025 g degraded about 95.96 and 96.8% dye, respectively. Such decrease/leveling in degradation with further increasing the catalyst quantity cause increase in solution opacity, which leads to a decrease in the penetration of the photon flux and ultimately decreases the photocatalytic degradation rate [58]. Similarly, 0.005 g of CuO NPs degraded 40.18% dye, while increasing catalyst loading to 0.010, 0.015, 0.020 and 0.025 g rate of photodegradation increases to 57.61, 68.22, 70.12 and 71.42%, respectively.
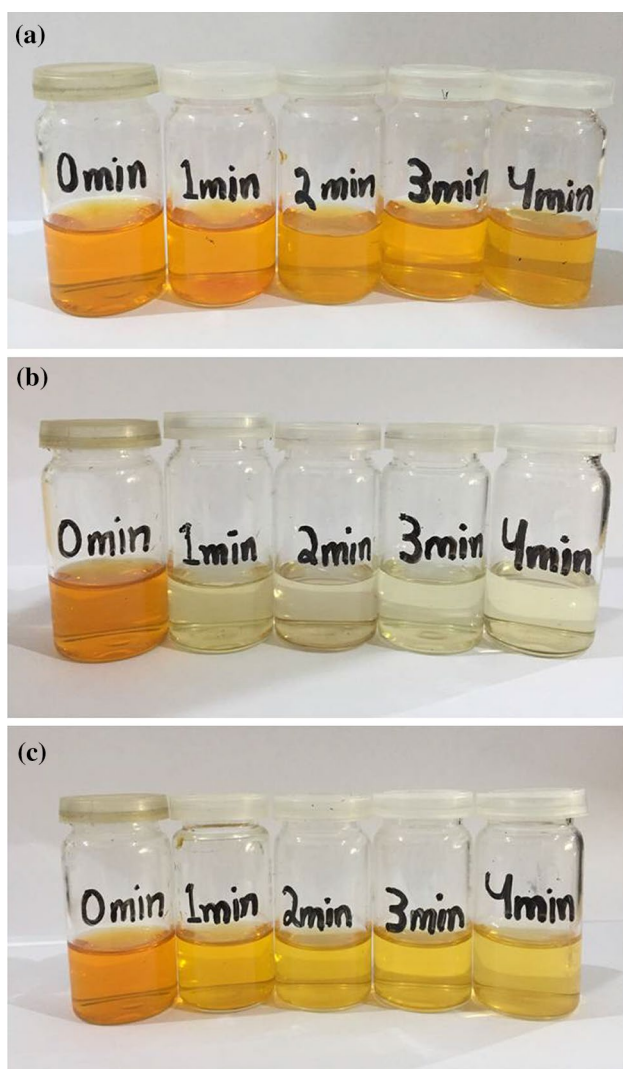
Fig. 10 Digital photograph of MO dye photodegraded in the presence of **a** NC, **b** CuO/NC NPs, **c** CuO NPs

3.8 Effect of initial dye concentration

Various industries discharge their effluents containing dyes at different concentrations and hence it is necessary to study the effect of initial dye concentration. The effect of initial dye concentration was evaluated by preparing different initial dye concentration solutions (10, 20, 30, 40 and 50 ppm)

keeping irradiation time (1 min) and catalyst dosage (0.015 g) constant. The % degradation of MO dye at various initial dye concentrations by CuO/NC NPs and CuO NPs is represented in Fig. 17. The results presented that the rate of dye degradation decreases as the initial concentration of MO dye is increased. The results show that CuO/NC NPs is very active and degraded dye efficiently at every concentration but the little change was observed as the initial concentration increases. It was found that at initial concentration of 10 ppm, the CuO/NC NPs degraded about 91.82% dye which decreased to 84.3% by increasing dye concentration to 50 ppm. Similarly, CuO NPs degraded 67.4% dye at 10 ppm, while at 50 ppm, it degraded 54.93% of the dye. This decrease in degrading efficiency with increasing dye concentration is due to the more adsorption of dye molecules on the surface of the catalyst. The adsorbed dye molecules may occupy the active sites, which absorb a significant amount of UV-light rather than a catalyst. Due to this phenomenon, less hydroxyl radical is produced and hence reduces the photocatalytic efficiency [58].

4 Conclusion

NC is stable support material and provides high surface area for the synthesis of CuO NPs on its surface. Supported NPs are well decorated and highly oxidized due to its high surface area, while unsupported are agglomerated and are thus less oxidized. The enhanced photocatalytic activity of CuO/NC NPs is attributed to the homogeneous dispersion of CuO NPs, which increase its surface area, and hence provide more photoactive sites for synergistic dye adsorption on the NC surface followed by its rapid photodegradation by supported CuO NPs. The less photocatalytic activity of CuO NPs is due to its less surface zeta potential charge, which results in agglomeration in dye solution/suspension. The good sustainability of recycled CuO/NC NPs is due to its easy recovering and easy washing. In tap water, the less photocatalytic activity of both the photocatalysts is due to various inorganic, organic and metallic ions present in tap water, which serve as competing species against the active sites of catalyst and hence reduce its activity. It was also found that the photodegradation of MO dye increases by increasing catalyst amount up to a certain limit and decreasing initial dye concentration.
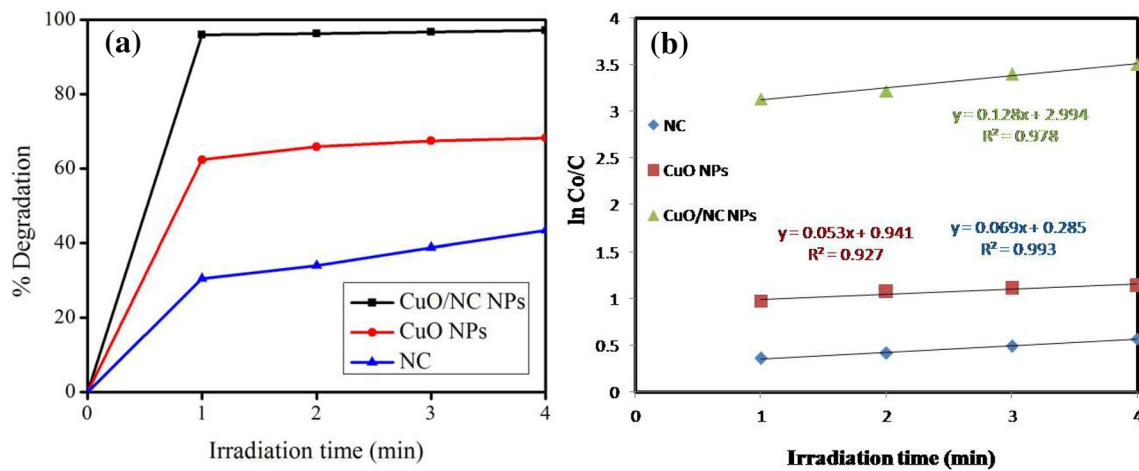
Fig. 11 a %degradation comparison of MO dye in the presence of NC, CuO/NC NPs and CuO NPs, **b** kinetic study of photodegradation reaction of MO

Table 1 Comparison of photodegradation efficiency of CuO/NC NPs with other photocatalysts reported in the literature

| Photocatalyst	Reaction conditions	MO dye degradation efficiency (%)	References
Cu_2O Micro–nano hierarchical structure	Dye concentration = 10 mg/L Dye amount = 5 mL Light source = visible	94.54% in 4 h	[50]
SnO_2 aerogel/rGO nanocomposite	Dye concentration = 1×10^{-5} M Catalyst amount = 1 mg mL^{-1} Light source = UV lamp	84% in 60 min	[51]
Ag NPs	Dye concentration = 2.5 mg/L Dye amount = 50 mL Light source = Xenon lamp	90% in 4 h	[52]
CuO/ZnO	Dye concentration = 5 ppm pH 6.8, Catalyst amount = 0.6 g Light source = UV-light	54.1% in 4 h	[53]
Si_{NWs}–Cu_{NPs}	Dye concentration = 20 ppm Dye amount = 20 mL Light source = visible (5 LEDS)	89% in 120 min	[54]
Xanthan gum/TiO_2 nanocomposite	Dye concentration = 30 ppm Dye amount = 100 mL Light source = visible	81% in 90 min	[55]
CuO/NC NPs	Dye concentration 30 ppm Catalyst amount = 0.015 g Light source = UV and visible	97.18% in 4 min (UV) 95.96% in 4 min (Vis)	Current study
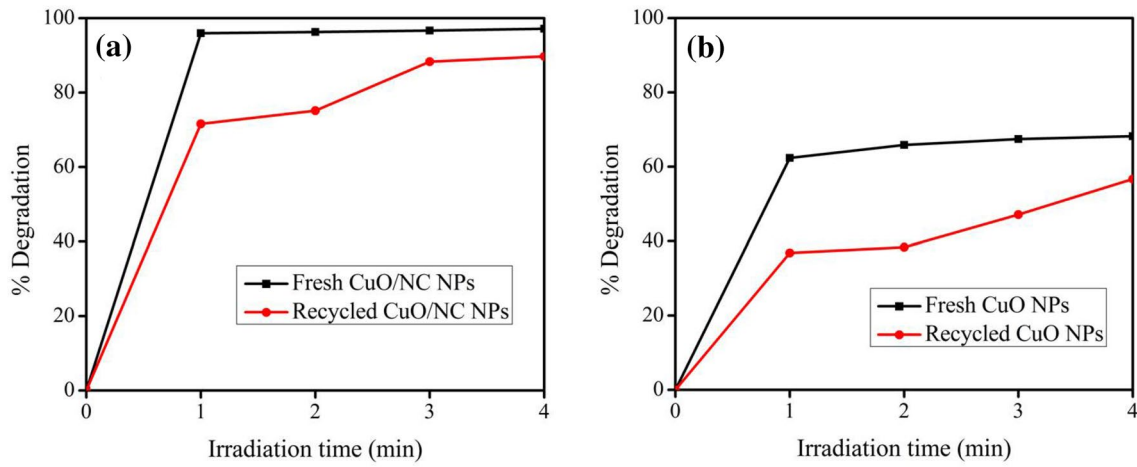
Fig. 12 Comparison of %degradation of MO dye photodegraded by fresh and recycled **a** CuO/NC NPs, **b** CuO NPs
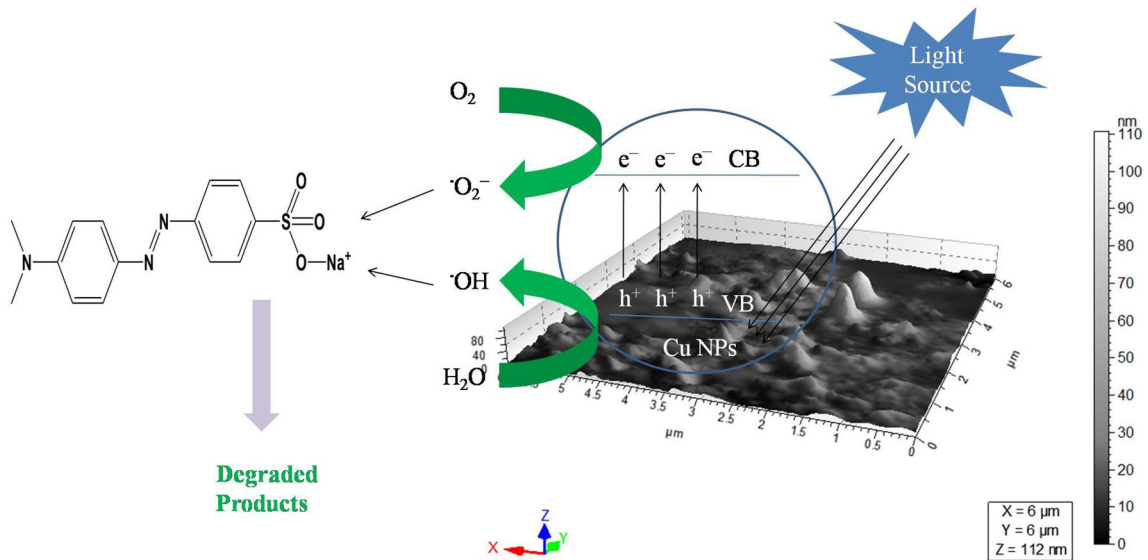

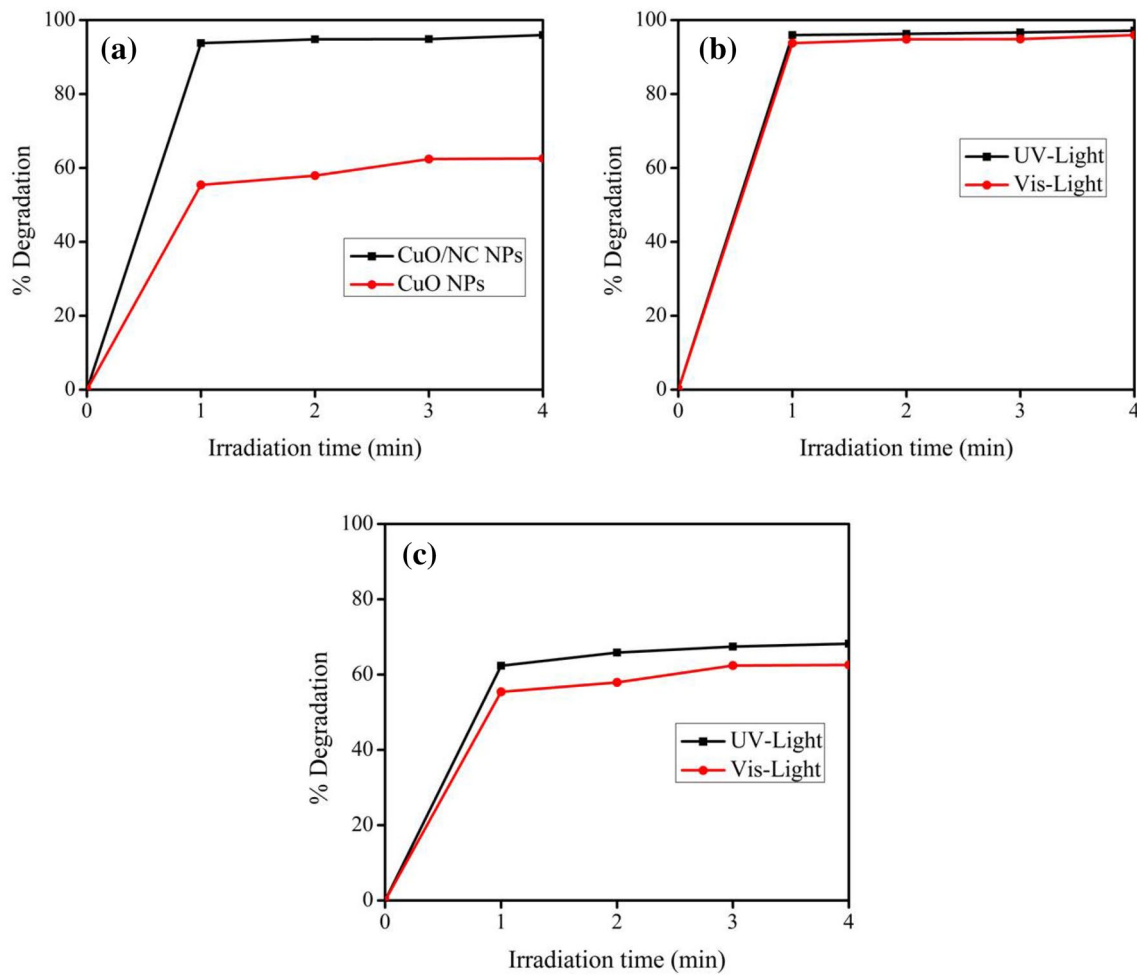**Fig. 13** Proposed mechanism for photodegradation of MO dye

Fig. 14 Comparison of % degradation of MO dye by **a** CuO/NC NPs and CuO NPs under visible light, **b** CuO/NC NPsNPs under UV and Visible light, **c** CuO NPs under UV and visible light
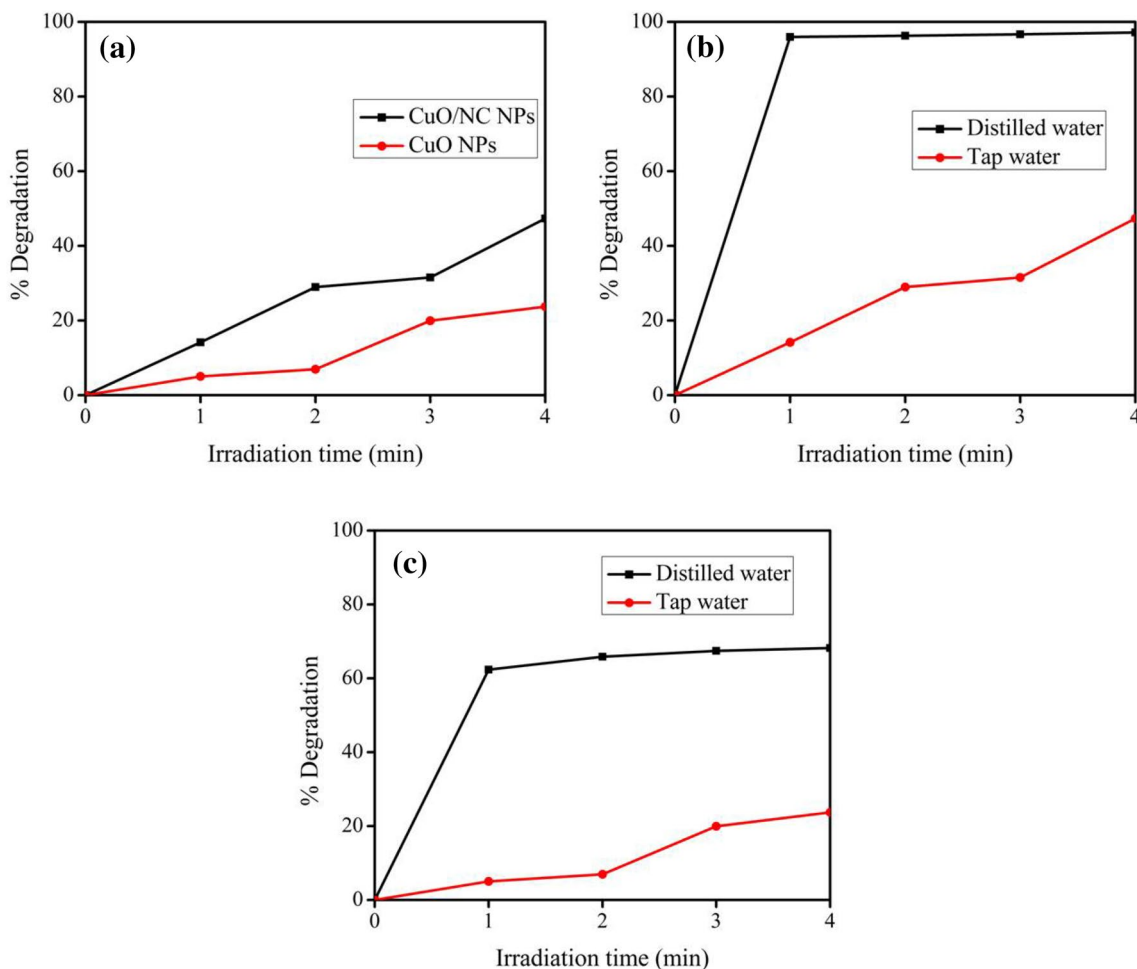
Fig. 15 % Degradation of MO dye under UV-light irradiation by **a** CuO/NC NPs in tap water, **b** CuO/NC NPs in distilled and tap water, **c** CuO NPs in distilled and tap water
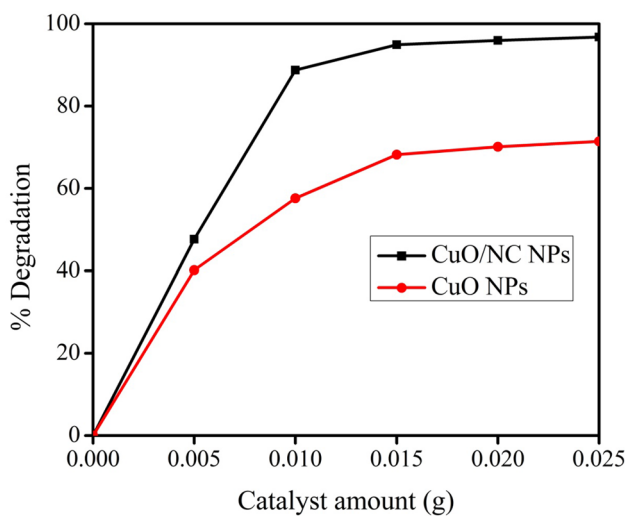

Fig. 16 Comparison of % degradation of MO dye photodegraded by the different quantities of CuO/NC NPs and CuO NPs
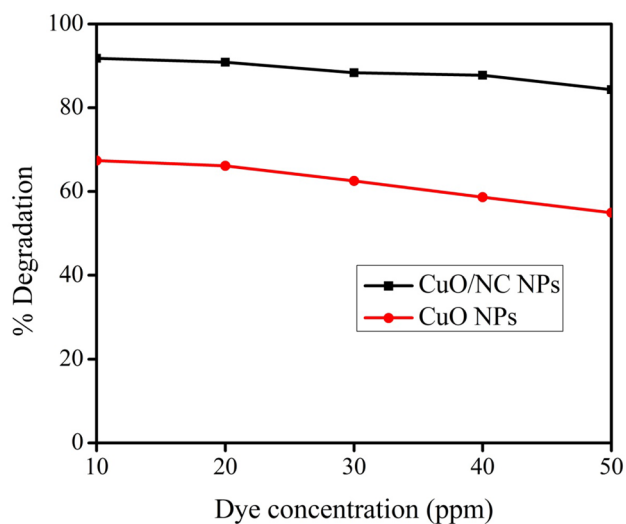

Fig. 17 % degradation of MO dye at various initial dye concentrations in the presence of CuO/NC NPs and CuO NPs

References

1. R. Arunadevi, B. Kavitha, M. Rajarajan, A. Suganthi, A. Jeyamurugan, Surf. Interfaces **10**, 32 (2018)
2. R.G. Saratale, G.D. Saratale, J.S. Chang, S.P. Govindwar, J. Taiwan Inst. Chem. Eng. **42**, 138 (2011)
3. I. Kazeminezhad, A. Sadollahkhani, Mater. Lett. **120**, 267 (2014)
4. H. Zhu, R. Jiang, L. Xiao, Y. Chang, Y. Guan, X. Li, G.Zeng, J. Hazard. Mater. **169**, 933 (2009)
5. S. Shahabuddin, R. Khanam, M. Khalid, N.M. Sarih, J.J. Ching, S. Mohamad, R. Saidur, Arab. J. Chem. **11**, 1000 (2018)
6. A. Kumar, G.Pandey, Mater. Sci. Eng. Int. J. **1**, 106 (2017)
7. K. Saeed, I. Khan, S.Y. Park, Desalin. Water Treat. **54**, 3146 (2015)
8. I. A.Elouinani, M. Boumanchar, Y. Zbair, A. Chhiti, F. Sahibeddine, M. Bentiss, Bensitel, J. Mater. Environ. Sci. **8**, 1301 (2017)
9. R. Tanwar, S. Kumar, U.K. Mandal, J. Photochem. Photobiol. A. Chem. **333**, 105 (2017)
10. K. Saeed, I. Khan, Turk. J. Chem. **41**, 391 (2017)
11. A.N. Ejhieh, M. Khorsandi, Desalination **262**, 79 (2010)
12. S.K. Kansal, S. Sood, A. Umar, S.K. Mehta, J. Alloys Compd. **581**, 392 (2013)
13. J. Marto, P.S. Marcos, T. Trindade, J.A. Labrincha, J. Hazard. Mater. **163**, 36 (2009)
14. J. Aliaga, N. Cifuentes, G. Gonzalez, C.S. Torres, E. Benavente, Catalysts **8**, 374 (2018)
15. K. Fischer, P. Schulz, I. Atanasov, A.A. Latif, I. Thomas, M. Kuhnert, A. Prager, J. Griebel, A. Schulze, Catalysts **8**, 376 (2018)
16. Y. Li, Q. Gu, X. Liu, M. Zhang, Mater. Sci. Forum **917**, 190 (2018)
17. V.K. Gupta, R. Jain, A. Mittal, M. Mathur, S. Sikarwar, J. Colloid Interface Sci. **309**, 464 (2007)
18. D. Yu, R. Cai, Z.Liu, Spectrochim. Acta A Mol. Biomol. Spectrosc. **60**, 1617 (2004)
19. W. Chomkitichai, J. Pama, P. Jaiyen, S. Pano, J. Ketwaraporn, P. Pookmanee, S. Phanichphant, P. Jansanthea, Appl. Mech. Mater. **886**, 138 (2019)
20. X. Liu, H. Zhai, P. Wang, Q. Zhang, Z. Wang, Y. Liu, Y. Dai, B. Huang, X. Qin, X. Zhang, Catal. Sci. Technol. **9**, 652 (2019)
21. M.R. Abhilash, G. Akshatha, S. Srikantaswamy, RSC Adv. **9**, 8557 (2019)
22. H. Gu, X. Chen, F. Chen, X. Zhou, Z. Parsaee, Ultrason. Sonochem. **41**, 109 (2018)
23. Z.A.M. Hir, P. Moradihamedani, A.H. Abdullah, M.A. Mohamed, Mater. Sci. Semicond. Process. **57**, 157 (2017)
24. A. Bhattacharyya, S. Kawi, M.B. Ray, Catal. Today **98**, 431 (2004)
25. M.P. Seabra, R.R. Pires, J.A. Labrincha, Chem. Eng. J. **171**, 692 (2011)
26. N. Zada, I. Khan, T. Shah, T. Gul, N. Khan, K. Saeed, Inorg. Nano-Met. Chem. **50**, 333 (2020)
27. S. Ali, Z. Li, S. Chen, A. Zada, I. Khan, I. Khan, W. Ali, S. Shaheen, Y. Qu, L. Jing, Catal. Today **335**, 557 (2019)
28. K. Saeed, M. Sadiq, I. Khan, S. Ullah, N. Ali, A. Khan, Appl. Water Sci. **8**, 60 (2018)
29. K. Mikami, Y. Kido, Y. Akaishi, A. Quitain, T. Kida, Sensors **19**, 211 (2019)
30. L. Lin, Y. Ma, Q. Xie, L. Wang, Q. Zhang, D.L. Peng, ACS Nano **11**, 6893 (2017)
31. J. Ha, Y.T. Kim, J. Choi, Chem. Sus. Chem. **13**, 419 (2020)
32. E. Alzahrani, R.A. Ahmed, Int. J. Electrochem. Sci. **11**, 47123 (2016)
33. A.P.A. Mary, A.T. Ansari, R. Subramanian, J. King Saud Univ. Sci. **31**, 1103 (2019)
34. A.N. Bnaerjee, S.W. Joo, Nanotechnology **22**, 365705 (2011)
35. Y. Cao, Y. Saygili, A. Ummadisingu, J. Teuscher, J. Luo, N. Pellet, F. Giordano, S.M. Zakeeruddin, J.E. Moser, M. Freitag, A. Hagfeldt, M. Gratzel, Nat. Commun. **8**, 15390 (2017)
36. M.N. Asl, N.M. Mahmodi, P. Teymouri, B. Shahmoradi, R. Rezaee, A.Maleki, Desalin. Water Treat. **57**, 1 (2016)
37. M. Batool, M.Z. Qureshi, F. Hashmi, N. Mehboob, W.M. Daoush, Asian J. Chem. **31**, 707 (2019)
38. C.R. Marcelo, G.A. Puiatti, M.A. Nascimento, A.F. Oliveira, R.P. Lopes, J. Nanomater. (2018). https://doi.org/10.1155/2018/4642038
39. T. Zhang, I.P.A.F. Souza, J. Xu, V.C. Almeida, T. Asefa, Nanomaterials **8**, 636 (2018)
40. M.S. Niasari, F. Davar, Mater. Lett. **63**, 441 (2009)
41. K. Saeed, I. Khan, T. Shah, S.Y. Park, Fiber Polym. **16**, 1870 (2015)
42. R. Gong, J. Ye, W. Dai, X. Yan, J. Hu, X. Hu, S. Li, H. Huang, Ind. Eng. Chem. Res. **52**, 14297 (2013)
43. Z. Hong, Y. Cao, J. Deng, Mater. Lett. **52**, 34 (2002)
44. Z. Li, Y. Xin, Z. Zhang, H. Wu, P. Wang, Sci. Rep. **5**, 10617 (2015)
45. Z. You, J.M. Beale, J.M. Foley, S. Roy, G.M. Odegard, Q. Dai, S.W. Goh, Constr. Build. Mater. **25**, 1072 (2011)
46. M.W. Ho, C.K. Lam, K. Lau, D.H.L. Ng, D.Hui, Compos. Struct. **75**, 415 (2006)
47. I. Khan, M. Sadiq, I. Khan, K. Saeed, Environ. Sci. Pollut. R. **26**, 5140 (2019)
48. F. Gao, H. Pang, S. Xu, Q. Lu, Chem. Commun. **24**, 3571 (2009)
49. L. Sun, X. Wu, M. Meng, X. Zhu, P.K. Chu, J. Phys. Chem. C **118**, 28063 (2014)
50. C. Dong, M. Zhong, T. Huang, M. Ma, D. Wortmann, M. Brajdic, I. Kelbassa, ACS Appl. Mater. Interfaces **3**, 4332 (2011)
51. T. Kim, V.G. Parale, H.N.R. Jung, Y. Kim, Z. Driss, D. Driss, A. Bouabidi, S. Euchy, H.H. Park, Nanomaterials **9**, 358 (2019)
52. H. Park, S.A. Hira, N. Muthuchamy, S. Park, K.H. Park, Nanomater. Nanotechnol. **9**, 1 (2019)
53. S.N.S. Jefri, A.H. Abdullah, E.N. Mohammad, Asian J. Green Chem. **3**, 271 (2019)
54. M.R.G. Robles, J.J.P. Bueno, C.S.A. Syllas, M.L.M. Lopez, F.M. Guerrero, MRS Adv. **3**, 3933 (2018)
55. Inamuddin, Int. J. Biol. Macromol. **121**, 1046 (2019)
56. K. Saeed, I. Khan, T. Gul, M.Sadiq, Appl. Water Sci. **7**, 3841 (2017)
57. N. Zada, K. Saeed, I. Khan, Appl. Water Sci. **10**, 40 (2020)
58. K.M. Reza, A.S.W. Kurny, F. Gulshan, Appl. Water Sci. **7**, 1569 (2017)